

PROPOSAL OF A NEW ALGORITHM OF THE THREE-COMPONENT DECOMPOSITION FOR AZIMUTHALLY INCLINED OBJECTS

PI No. 231

Shunichi Kusano¹, Manabu Watanabe², Motoyuki Sato³

¹ Graduate School of Environmental Studies, Tohoku University

^{2,3} Center for NorthEast Asian Studies, Tohoku University

^{1,2,3} Kawauchi 41, Aoba, Sendai, Miyagi, Japan

^{1,2,3} TEL & FAX +81-(0)22-795-6074

¹ kusano@cneas.tohoku.ac.jp

² mwatana@cneas.tohoku.ac.jp

³ sato@cneas.tohoku.ac.jp

Abstract

In this paper, we propose a new decomposition based on the three-component decomposition so that it can be applied to targets with azimuth inclination. The proposed method employs rotations of the scattering matrix. However, the rotation process is embedded to the models for double bounce and surface scattering, different from the deorientation. In addition, the new algorithm applies the circular polarization basis due to its simplicity to handle the rotation. Applying the proposed method and comparing it to the three-component decomposition, it is confirmed that azimuthally tilted slopes and skew-oriented buildings are more accurately decomposed into their corresponding scattering mechanisms.

1. INTRODUCTION

Decomposition techniques applied to polarimetric SAR data are quite important to interpret and understand polarimetric SAS images [1]-[4]. The three-component decomposition has been widely employed for polarimetric SAR data analysis, because it is simple and resulting images are easy to be understood. However, its applicable range is limited to the area where reflection symmetry condition is satisfied such as forests and grasslands. Consequently, if we apply it to the area where reflection symmetry condition does not hold, unreasonable results appear. For example, skew-oriented buildings and azimuthally inclined slopes look volume scattering by the three-component decomposition. This is because they have high stable HV reflections. In order to overcome this limitation, a new decomposition is proposed in this paper. The models of the scattering matrix to represent each scattering mechanism are modified so that they include rotation angles along the line of sight. Targets with azimuth inclinations can be represented by those models. Furthermore, the models are represented by the circular polarization basis due to its simplicity of the expression

for the rotation. This scheme is essentially the same as deorientation [5]-[8] that employs the rotation of scattering matrices. The difference between the proposed method and the deorientation is whether the rotation process is embedded to the models. The models which are newly constructed and the entire process for the proposed method are described in detail in the second and the third sections. The fourth section provides decomposition results and their validations by comparing the three-component decomposition and the proposed method.

2. MODELS

In this section, the polarimetric scattering properties are described and modeled for two targets, i.e., azimuthally tilted terrain slopes and skew-oriented buildings. In other word, we aim at the generalization of the models for surface and double-bounce scattering.

First, we start from surface scattering. We assume that surface scattering is represented as first-order Bragg scattering, as assumed in the three-component decomposition. The scattering matrix is described as

$$S_{bragg} = \begin{bmatrix} 1 & 0 \\ 0 & \beta \end{bmatrix} \quad (1)$$

where β is real and normalized by HH. If the normal to the ground is included in the incident plane, the cross-polarization reflection is not caused as described in (1). The property had been well studied, if the normal deviates from the incident plane, in other words, if the ground slope is tilted azimuthally [9]. Letting the rotation angle be θ , the scattering matrix for the azimuthally tilted ground surface is represented as

$$S_{az_tilted} = \begin{bmatrix} \cos \theta & -\sin \theta \\ \sin \theta & \cos \theta \end{bmatrix} \begin{bmatrix} 1 & 0 \\ 0 & \beta \end{bmatrix} \begin{bmatrix} \cos \theta & \sin \theta \\ -\sin \theta & \cos \theta \end{bmatrix} \quad (2)$$

From the geometry, the PO angle is expressed as [9]

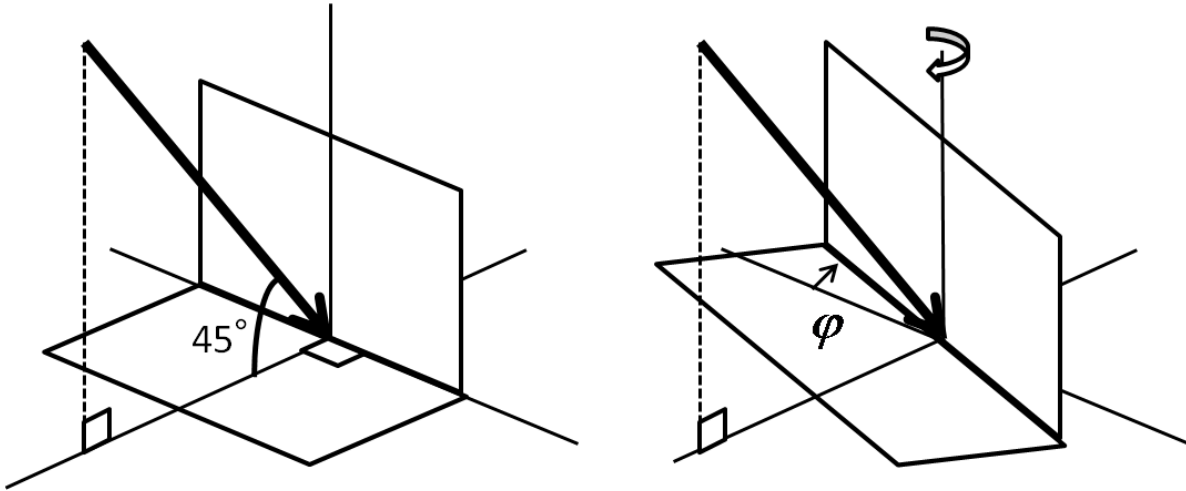


Fig. 1 Simulated configuration for an azimuthally rotated dihedral corner reflector

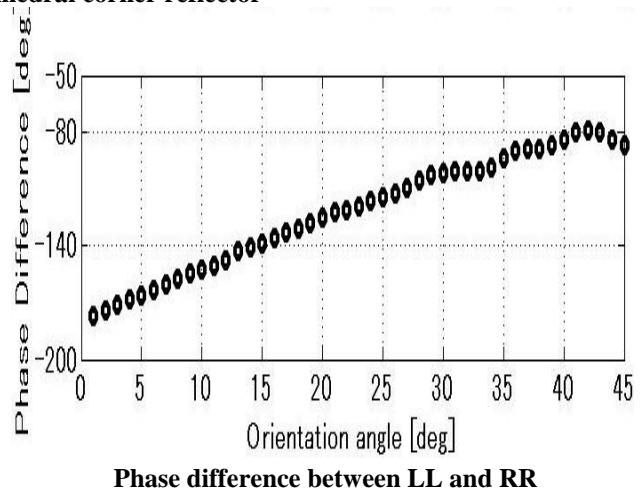
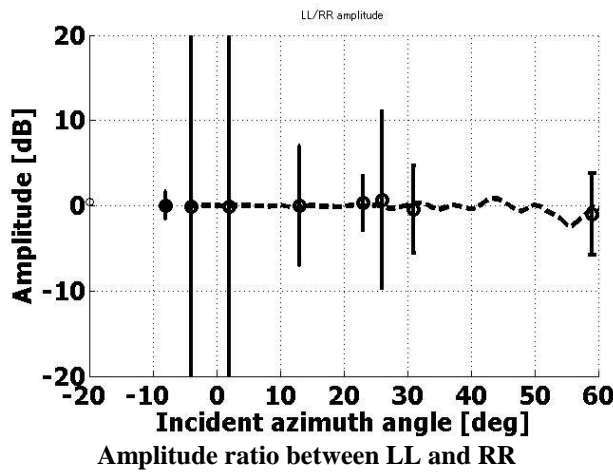


Fig. 2 Observed and simulated results as orientation angle of buildings changes

$$\tan \theta = \frac{\tan \omega}{-\tan \gamma \cos \phi + \sin \phi} \quad (3)$$

where $\tan \omega$ is azimuth slope, $\tan \gamma$ is range slope, and ϕ is incident angle. The PO angle can be estimated accurately, by employing the circular polarization basis, as [9]

$$\theta = \left[\text{Arg} \left(\left\langle S_{RR} S_{LL}^* \right\rangle \right) + \pi \right] / 4 \quad (4)$$

This approach can be easily expanded to other flat surfaces such as roofs and walls of buildings. Consequently, the scattering matrix model is represented by (2) for the azimuthally tilted surface.

Next, skew-oriented buildings are considered as the model for general dihedral structures. These targets are known as reflectors causing a strong cross-polarization [10][11]. In order to investigate the polarimetric response of skew-oriented buildings more carefully, we conducted a numerical simulation by the method of moment [12]. The simulation configuration is shown in Fig. 1. The target is a dihedral corner reflector whose faces are regarded as a

wall of a building and the ground, respectively. The side length is 16.6λ and the incident angle is 45 degree. The polarimetric response is calculated with respect to a variety of orientation angles. The results are shown in Fig. 2. The amplitude ratio between LL and RR is 1 up to around 45 degree of orientation angle and the phase difference between them shows a linear change up to around 40 degree. From these results, we built a scattering matrix model for skew-oriented buildings in the circular polarization basis as

$$S_{skew_building} = \begin{bmatrix} 1 & \gamma \\ \gamma & e^{j\phi} \end{bmatrix} \quad (5)$$

where all elements are normalized by LL. The ratio of LR to LL is γ and ϕ is the phase difference between LL and RR. The amplitude of γ is found to be smaller than 1 from the simulation and the observation of the real data. Furthermore, we have noticed that (5) is similar to the scattering matrix of the double-bounce used in the three-component decomposition by adding the rotation, that is

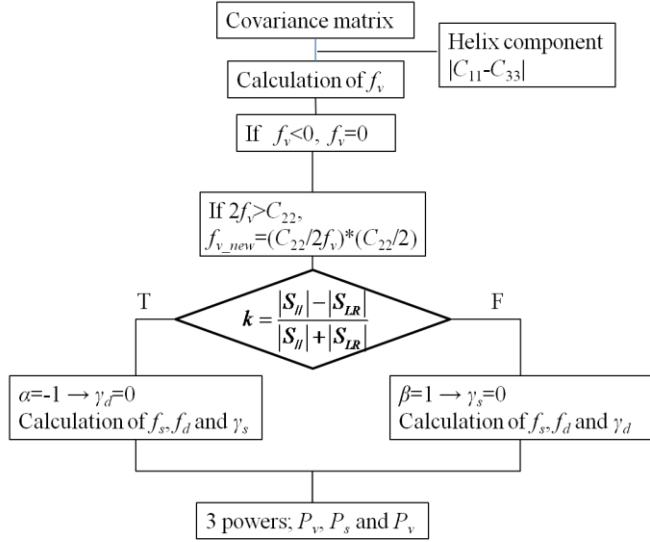


Fig. 3 Flowchar of the proposed method

$$\begin{aligned}
 S_{double}^{(LR)} &= \mathbf{U}_c \mathbf{R} \begin{bmatrix} 1 & 0 \\ 0 & \alpha \end{bmatrix} \mathbf{R}^{-1} \mathbf{U}_c^\dagger \\
 &= \frac{1}{2} \begin{bmatrix} (1-\alpha)e^{j2\theta} & (1+\alpha)/j \\ (1+\alpha)/j & (\alpha-1)e^{-j2\theta} \end{bmatrix} \\
 &= S_{LL} \begin{bmatrix} 1 & S_{LR}/S_{LL} \\ S_{LR}/S_{LL} & -e^{-j4\theta} \end{bmatrix}
 \end{aligned} \quad (6)$$

where \mathbf{U}_c and \mathbf{R} are the transformation matrix from the linear to the circular polarization basis and the rotation matrix, respectively. This fact agrees with what was mentioned in [10]. Hence, we assume that the scattering matrix for skew-oriented buildings as (5).

3. PROPOSED METHOD

A new decomposition based on the three-component decomposition is constructed and we show how the solutions are derived in this section. We have the new surface and double-bounce scattering models applicable to azimuthally inclined cases, respectively. In the circular polarization basis, they are represented as

$$S_{double} = \begin{bmatrix} e^{j2\theta_d} & \gamma_d \\ \gamma_d & -e^{-j2\theta_d} \end{bmatrix}. \quad (7)$$

$$S_{surface} = \begin{bmatrix} \gamma_s e^{j2\theta_s} & 1 \\ 1 & -\gamma_s e^{-j2\theta_s} \end{bmatrix}. \quad (8)$$

where γ_d is $j(1+\alpha)/(1-\alpha)$, γ_s is $(1-\beta)/j(1+\beta)$, θ_d and θ_s are the polarization orientation angles for double-bounce and surface scattering, respectively. For volume scattering, we apply the randomly oriented dipole model with constant probability density function. The covariance matrix for volume scattering in the circular polarization basis is modeled as

$$C_v = \begin{bmatrix} 1 & 0 & 0 \\ 0 & 2 & 0 \\ 0 & 0 & 1 \end{bmatrix}. \quad (9)$$

Finally, an observed covariance matrix is expressed as the linear combination of these matrices as

$$\begin{aligned}
 C &= \begin{bmatrix} \langle S_{LL} S_{LL}^* \rangle & \sqrt{2} \langle S_{LL} S_{LR}^* \rangle & \langle S_{LL} S_{RR}^* \rangle \\ \sqrt{2} \langle S_{LR} S_{LL}^* \rangle & 2 \langle S_{LR} S_{LR}^* \rangle & \sqrt{2} \langle S_{LR} S_{RR}^* \rangle \\ \langle S_{RR} S_{LL}^* \rangle & \sqrt{2} \langle S_{RR} S_{LR}^* \rangle & \langle S_{RR} S_{RR}^* \rangle \end{bmatrix} \\
 &= f_s C_{surface} + f_d C_{double} + f_v C_{volume}
 \end{aligned} \quad (10)$$

where f_s , f_d and f_v are coefficients for surface, double-bounce and volume scattering, respectively. The power of each is calculated with the following equations

$$P_s = 2f_s (1 + |\gamma_s|^2). \quad (11a)$$

$$P_d = 2f_d (1 + |\gamma_d|^2). \quad (11b)$$

$$P_v = 4f_v. \quad (11c)$$

Next, we show how the unknowns are fixed. Each element in an observed covariance matrix is written down as

$$C_{co-pol} = f_d + |\gamma_s|^2 f_s + f_v. \quad (12a)$$

$$C_{22} = 2|\gamma_d|^2 f_d + 2f_s + 2f_v. \quad (12b)$$

$$C_{13} = -f_d e^{j4\theta_d} - |\gamma_s|^2 f_s e^{j4\theta_s}. \quad (12c)$$

$$C_{12} = \sqrt{2}\gamma_d^* e^{j2\theta_d} f_d + \sqrt{2}\gamma_s e^{j2\theta_s} f_s. \quad (12d)$$

$$C_{23} = -\sqrt{2}\gamma_d e^{j2\theta_d} f_d - \sqrt{2}\gamma_s^* e^{j2\theta_s} f_s. \quad (12e)$$

For a simple description, C_{co-pol} is used in place of C_{11} and C_{33} . We have five equations and seven unknowns here. Several assumptions are needed to solve these equations. The first assumption is the same as that used in the three-component decomposition [2]. The dominant scattering process is judged between surface scattering and double-bounce. If surface scattering is dominant, α is assumed to be -1, i.e., $\gamma_d = 0$. If double-bounce scattering is dominant, β is assumed to be +1, i.e., $\gamma_s = 0$. In the the three-component decomposition, the sign of $\text{Re}(\langle S_{hh} S_{vv}^* \rangle)$ is used as the discriminator. The small letters in the subscripts denotes the residual after the removal of f_v . Instead of this, we utilize the following discriminator.

$$k = \frac{|S_{//}| - |S_{LR}|}{|S_{//}| + |S_{LR}|}. \quad (13)$$

where $|S_{//}|$ is the average of $|S_{LL}|$ and $|S_{RR}|$. If k is over 0, we think that double-bounce is dominant, and *vice versa*. This criterion has the same meaning as that used in the three-component decomposition, if the deorientation is done. The second assumption is about the PO angle, θ .

We assume that the PO angles for surface and double-bounce scattering are the same as the following.

$$\theta = \theta_d = \theta_s. \quad (14)$$

This condition is considered to be valid, if there is one dominant scattering mechanism in a local window. Under this condition, the minor scattering mechanism is regarded negligible, then, it is relatively acceptable that the PO angle of minor scattering is determined to be the same as that of the major scattering process. Hence, it should be noted that it needs attentions to apply this assumption to urban areas where there is a high density of small houses.

All the variables are determined by applying the two assumptions above. First, the PO angle is determined from (12c) and (14). Then, the coefficient of volume scattering is easily determined by

$$f_v = C_{co-pol} - |C_{13}|. \quad (15)$$

After removal of f_v , the dominant scattering process is determined as between surface and double-bounce scattering by the first assumption. It should be noted that (12d) and (12e) are equal, if (14) is valid, since $C_{12} = -e^{j4\theta} C_{23}^*$ is met. By the second assumption, the remainings are solved as

surface scattering dominant,

$$\gamma_s = \frac{C_{12}}{\sqrt{2}C'_{22}} e^{-j2\theta}, \gamma_d = 0$$

$$f_s = C'_{22}, f_d = C'_{co-pol} - \frac{|C_{12}|^2}{2|C'_{22}|}.$$

double-bounce dominant,

$$\gamma_s = 0, \gamma_d = \frac{C_{12}^*}{\sqrt{2}C'_{co-pol}}$$

$$f_s = C'_{22} - \frac{|C_{12}|^2}{2|C'_{co-pol}|}, f_d = C'_{co-pol}.$$

where $C'_{co-pol} = C_{co-pol} - f_v$ and $C'_{22} = C_{22} / 2 - f_v$. Finally, the process flow for the proposed method is shown in Fig. 3.

4. RESULTS AND VALIDATIONS

The proposed methods are validated in this section. The proposed method improves both surface and double-bounce scattering. Thus, we examine their improvements separately. First, double-bounce scattering is examined by employing the L-band SAR data acquired by ALOS/PALSAR [13]. The data were taken over Sendai/Japan. Figure 4(a) shows the aerial photo of the selected area. From this image, it is obvious that buildings are built densely except for the left part of the image. The multi-look processing was done to the acquired data. We show the resulting color-composite images processed by

the three-component decomposition and the proposed method, respectively in Fig. 4(b) and 4(c). The range direction is from the left to the right. Significant differences appear at the center and the right part of the images that double bounce in the proposed method looks dominant than the three-component decomposition. However, there is not much difference at the mid-center of both images, though we have skew-oriented buildings there. This is because the buildings are relatively small, dense and their orientations are not constant. Thus, the scattering mechanisms are quite complex and the second assumption we employed does not hold in the area. In order to observe the results quantitatively, the left figure of Fig. 6 illustrates the relation between the orientation angle of the buildings and the power ratio of double-bounce with respect to both methods. The power ratio of each scattering process p_x is calculated as

$$p_x = \frac{P_x}{P_d + P_s + P_v}. \quad (17)$$

where $x=d$ or s or v . The power ratios by the both methods are above 0.9 at several degrees and decrease gradually as the orientation angle increases. The degree of decrease for the proposed method is milder than that for the three-component decomposition. The difference is about 0.2 in the range above 10 degree. Finally, the power ratio is kept at around 0.4 at 30 degree by the proposed method, though it is only 0.2 by the three-component decomposition.

Next, we examine the improvement of surface scattering. The data taken over Mt. Fuji by L-band of PALSAR/ALOS is chosen for the validation. The ground slope around the summit is less-vegetated and relatively smooth, and mostly spreads isotropically from the summit. Figure 5 shows the power ratio of surface scattering calculated by (17) with respect to the three-component decomposition and the proposed method, respectively. The azimuthally tilted mountain slope which is our main target is distributed around the top and bottom part of the summit. From the images, we can see that the power ratio of surface scattering is larger in the proposed method. Around the area, the azimuth tilt angle of the slope is estimated to be around 25-30 degree from the DEM [14]. The histogram for the power ratio of the surface scattering calculated in the area are shown in the right figure of Fig. 6 comparing the three-component decomposition and the proposed method. From the image, we can see the increase of the power ratio from 0.55 to 0.77 due to the application of the proposed method. These results show the usefulness of the proposed method.

5. CONCLUSION

The method for an improvement of the three-component decomposition was proposed to overcome the problem that azimuthally inclined objects look volume scattering in the three-component decomposition. The new method

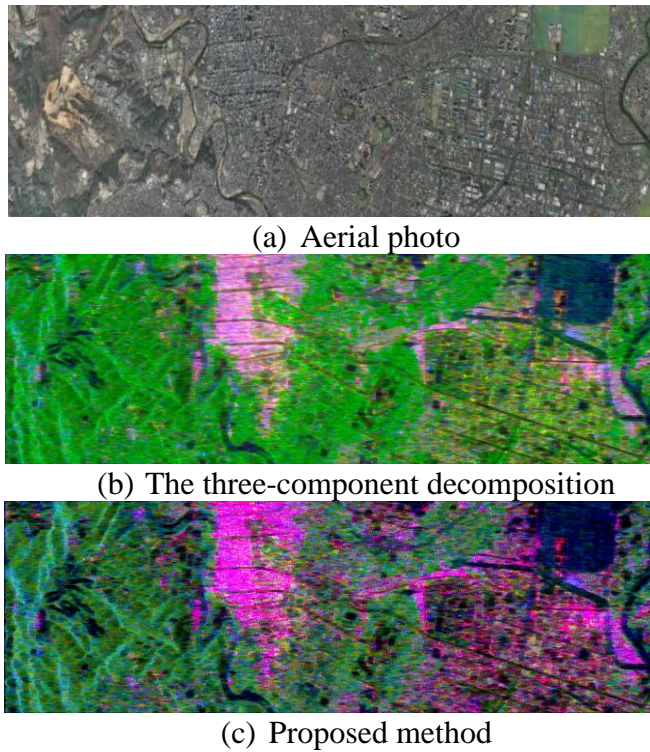


Fig. 4 Analyzed areas.

Red: Double-bounce
Blue: Surface scattering
Green: Volume scattering

introduced the rotation along the line of sight to the models used in the three-component decomposition so that they include the azimuth inclination. The method was applied to real data and it was confirmed that the power ratio of surface scattering and double-bounce scattering returned from the azimuthally inclined objects such as azimuthally tilted ground slopes and skew-oriented buildings increases, respectively. Consequently, the proposed methods provide a means of obtaining better observations of polarimetric SAR images.

6. ACKNOWLEDGEMENT

We appreciate JAXA to provide the dataset used for the validations in this paper.

Also, we would like to thank JSPS, because this work was supported by JSPS Grant-in -Aid for Scientific Research (S) 18106008.

7. REFERENCES

- [1] S. R. Cloude and E. Pottier, "A review of target decomposition theorems in radar polarimetry," *IEEE Trans. Geosci. Remote Sens.*, vol. 34, no. 2, pp. 498–518, Mar. 1996.
- [2] A. Freeman and S. L. Durden, "A three-component

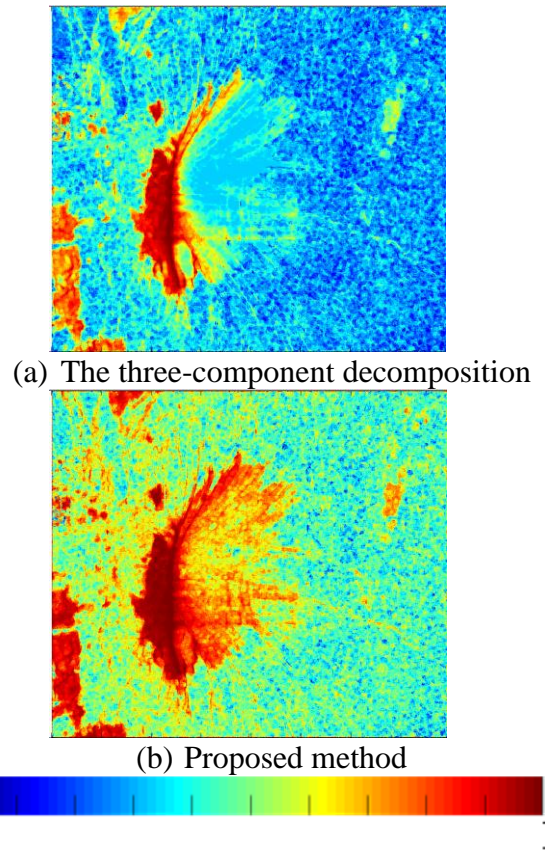


Fig. 5 Power ratios of surface scattering.

scattering model for polarimetric SAR data," *IEEE Trans. Geosci. Remote Sens.*, vol. 36, no. 3, pp. 963–973, May 1998.

- [3] W. L. Cameron , N. Youssef, and L. K. Leung, "Simulated polarimetric signatures of primitive geometrical shapes," *IEEE Trans. Geosci. Remote Sens.*, vol. 34, no. 3, pp. 793-803, May 1996.
- [4] Y. Yamaguchi, T. Moriyama, M. Ishido, and H. Yamada, "Four-component scattering model for polarimetric SAR image decomposition," *IEEE Trans. Geosci. Remote Sens.*, vol. 43, no. 8, pp. 1699–1706, Aug. 2005.
- [5] Feng Xu, and Ya-Qiu Jun, "Deorientation theory of polarimetric scattering targets and application to terrain surface classification," *IEEE Trans. Geosci. Remote Sens.*, vol. 43, no. 10, pp. 2351-2364, Oct. 2005.
- [6] Jong-Sen Lee, Dale L. Schuler, and Thomas L. Ainsworth, "Polarimetric SAR data compensation for terrain azimuth slope variation," *IEEE Trans. Geosci. Remote Sens.*, vol. 38, no. 5, pp. 2153–2163, Sep. 2000.
- [7] Jong-Sen Lee, Thomas L. Ainsworth, and Kun-Shan Chen, "The effect of orientation angle compensation on polarimetric target decompositions," in *Proc. IGARSS*, Cape Town, South Africa, Jul. 2009, pp.

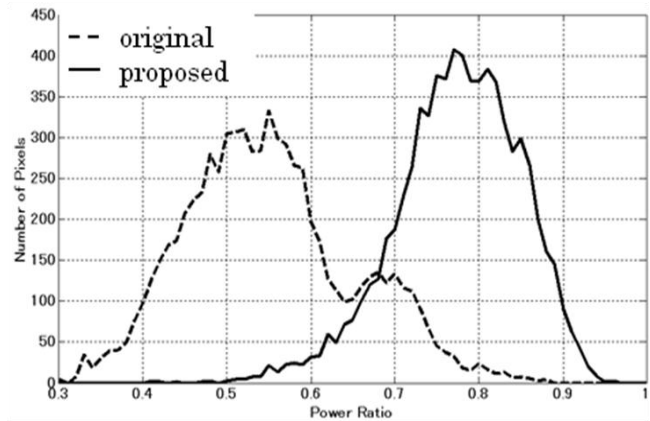
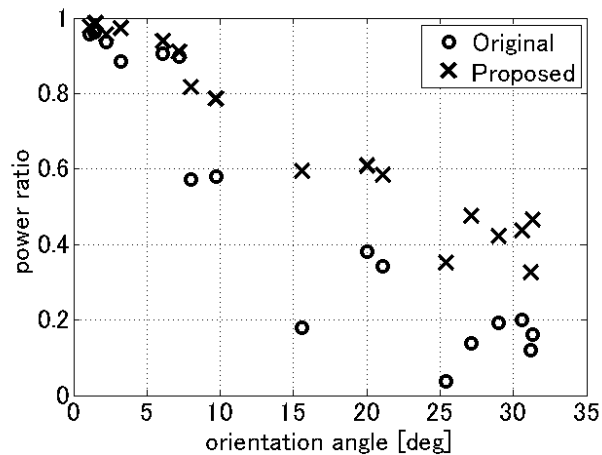


Fig. 6 Power ratios of the double bounce and the surface scattering in the analyzed areas. The left image shows the relation between the double-bounce power ratio and orientation angle of buildings. The right image shows the power ratio of the surface scattering.

IV-849–IV-852.

- [8] Y. Yamaguchi, A. Sato, R. Sato, H. Yamada, W. M. Boerner, “Four-component scattering power decomposition with rotation of coherency matrix,” *Proc. of IGARSS10*, Honolulu, HI, Jul. 2010.
- [9] J. S. Lee, D. Schuler, T. L. Ainsworth, E. Krogager, D. Kasilingam, and W. M. Boerner, “On the estimation of radar polarization orientation shifts induced by terrain slopes,” *IEEE Trans. Geosci. Remote Sens.*, vol. 40, no. 1, pp. 30–41, Jan. 2002.
- [10] H. Kimura, “Radar polarization orientation shifts in built-up areas,” *IEEE Geosci. Remote Sens. Lett.*, vol. 5, no. 2, pp. 217–221, Apr. 2008.
- [11] K. Iribe, M. Sato, “Analysis of polarization orientation angle shifts by artificial structures,” *IEEE Geosci. Remote Sens.*, vol. 45, no. 11, pp. 3417–3425, Nov. 2007.
- [12] R. F. Harrington, “Field computation of moment method,” Macmillan, 1961 .
- [13] [Online] http://www.eorc.jaxa.jp/ALOS/Pi-SAR/about_pisar.html
- [14] [Online] http://dds.cr.usgs.gov/srtm/version2_1